51st AIAA Aerospace Sciences Meeting
7-10 Jan 2013, Grapevine, TX
AIAA-2013-0717

Aero-Optical Mitigation of Shocks Around Turrets at Transonic Speeds Using Passive Flow Control

Stanislav Gordeyev[1], Robert Burns[2], Eric Jumper[3]
University of Notre Dame, Notre Dame, Indiana, 46545

Sivaram Gogineni[4],
Spectral Energies, LLC, Dayton, OH 45431

Michael Paul[5] and Donald Wittich[6]
Air Force Research Laboratory, Directed Energy Directorate, Kirtland AFB, NM 87117

Experimental studies of the aero-optical effects around a partially-protruding cylindrical turret for a range of incoming transonic Mach numbers are presented and discussed. Spatially-temporally resolved wavefronts were collected using a high-speed Shack-Hartmann sensor and flow visualization was performed with a Schlieren system. Different flow regimes with a local shock, either a steady or an unsteady one, were described for the baseline case and the shock dynamics was found to be sensitive to a local flow speed. In addition, several passive flow control devices, consisted of a single spanwise row of vertically-placed small-diameter pins or porous screens, were tested in order to mitigate detrimental unsteady-shock-related aero-optical effects. It was found that passive flow control devices with large blockage values slowed the flow near the cylinder surface down to subsonic speeds by introducing total pressure losses in the wall region upstream of the cylinder, thus eliminating the shock formation over a wide range of transonic Mach numbers and significantly improving aero-optical environment at some elevation angles.

I. Introduction

FOR many practical applications which require sending or transmitting a laser beam from an airborne platform, turrets provide convenient means to point-and-steer the laser beam. However, a turret bluff-body shape creates a complex turbulent flow around it [1]. For Mach numbers larger than 0.3, these turbulent fluctuations create unsteady density fluctuations around the turret and impose detrimental aero-optical effects on the outgoing beam. These aero-optical effects [2,3] result in unwanted unsteady beam defocus and jitter on the target, disrupting a high-speed optical link in free-space laser-based communication systems, for instance.

When the flow is subsonic everywhere around the turret, essential flow features and related aero-optical distortions have being extensively studied in last few years and fairly well-understood [1,3-7]. But for incoming Mach numbers larger than approximately 0.55, the flow on top of the hemisphere-on-cylinder turret becomes supersonic, with a resulting local shock present on top of the turret [1,5]. The shock creates strong unsteady density gradients in the flow and promotes an earlier separation of the flow off the turret. All these shock-related features add additional aero-optical distortions to the outgoing beam [5,8]. Figure 1 shows results of the numerical simulations of the flow for a hemispherical turret for incoming Mach numbers of M = 0.7 and 0.9. These results demonstrate additional features in the flow around 3-dimensional turrets at transonic speeds, such as the formation

[1]Research Associate Professor, Department of Mechanical and Aerospace Engineering, Hessert Laboratory for Aerospace Research, Notre Dame, IN 46556, Senior AIAA Member.
[2]Graduate Student, Department of Aerospace and Mechanical Engineering, Hessert Laboratory for Aerospace Research.
[3]Professor, Department of Mechanical and Aerospace Engineering, Hessert Laboratory for Aerospace Research, Notre Dame, IN 46556, AIAA Fellow.
[4]President, 5100 Springfield St. Suite 301, Dayton OH 45431, Senior AIAA Member.
[5]Aero-Optics Engineer, Laser Division, 3550 Aberdeen Ave SE
[6]Aerospace Engineer, Laser Division, 3550 Aberdeen Ave SE

of the supersonic flow region and the ending shock, the shock extent and the angle depending on the incoming Mach number, and the separation is prematurely forced by the shock, compared to the subsonic separation.

Different flow control approaches were investigated to order to mitigate aero-optical effects caused by turrets at subsonic speeds [1,6,7], but investigation of shock manipulation to improve aero-optical environment around turrets at transonic or supersonic speeds is largely lacking.

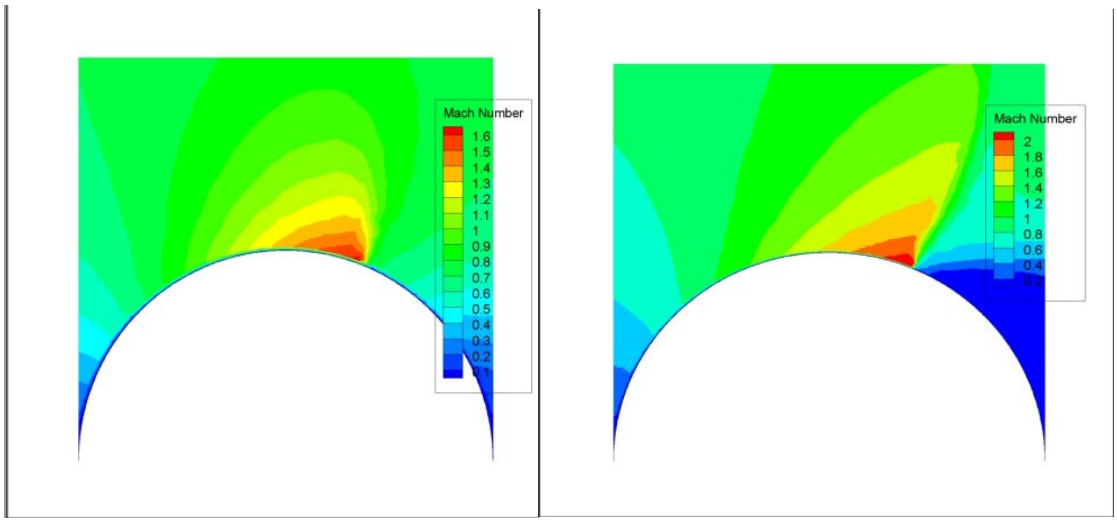

Figure 1. 3-D flow simulations over the hemisphere-on-cylinder turret for the incoming Mach number of 0.7 (left plot) and 0.9 (right plot).

The flow around the turret is dominated by two factors. The first factor is a streamwise surface curvature, which creates streamwise pressure gradients and ultimately is responsible for the flow separation at the aft of the turret. The second factor is the surface curvature in the spanwise direction, which creates spanwise shearing forces and responsible for the three-dimensionality of the wake and the formation of the necklace and the horn vortices around the turret. As the shock formation is governed mostly by the streamwise pressure gradients, the flow around a two-dimensional turret has been experimentally studied to better understand the flow dynamics and related aero-optical effects due to the presence of the local shock on the turret and to properly test different flow control strategies. The subsonic flow around the two-dimensional turret was shown to have most essential flow features, as around three-dimensional turrets [1,9] and was found to provide a convenient platform to understand the nature of aero-optical distortions around turrets, as well as to test different flow mitigation approaches [10-12].

This paper presents recent experimental investigation of the flow topology and related aero-optical effects around a partially-protruding cylinder over a wide range of incoming transonic Mach numbers, for both the baseline case and for several passive flow control devices placed upstream of the cylinder. With some preliminary qualitative flow studies given in Section II, Section III describes the experimental set-up and data reduction procedure. Detailed discussion of results for both the baseline and passive flow-control cases is provided in Section IV. Finally, conclusions and discussion are given in Section V.

II. Preliminary Studies

To study how a curvature in the streamwise direction affects the flow feature over a range of transonic speeds, series of the preliminary flow visualizations were performed over a cylindrical “slice” with a 100-mm diameter curvature and 25 mm high, mounted in an optical test section of a transonic in-draft tunnel at University of Notre Dame, see Figure 2. The facilities were described in detail in Gordeyev at al. [13] and an interested reader is referred to this reference for a complete discussion. To achieve different incoming Mach numbers, the flow in the tunnel test section was driven by up to two vacuum pumps with variable valve settings between the test section and the vacuum plenum. The test section height was 100 mm and the width was 100 mm. The flow over the partially-protruding cylindrical “slice” at different speeds was investigated with Schlieren system. Results of the flow visualization at different incoming Mach Numbers are presented in Figure 3. At low incoming Mach numbers, the flow over the cylindrical “slice” was subsonic everywhere and the separation occurred at approximately 120 degrees. The separation angle was very similar to the separation angle observed at 3-dimensional hemisphere-on-

cylinder turrets [1]. When the incoming Mach number approached M = 0.46, the flow on top of the cylindrical "slice" became supersonic with an ending shock, see Figure 3, upper left plot. When the incoming Mach number increased further, the shock became stronger, extended away from the cylinder and became more oblique, see Figure 3, top right and bottom left plots. The shock forced a premature flow separation and the separation region became larger. At some even larger Mach number, the supersonic shock reached the opposite tunnel wall and the flow choked. Further increase of the Mach number intensified the shock and moved it further downstream, see Figure 3, bottom right plot.

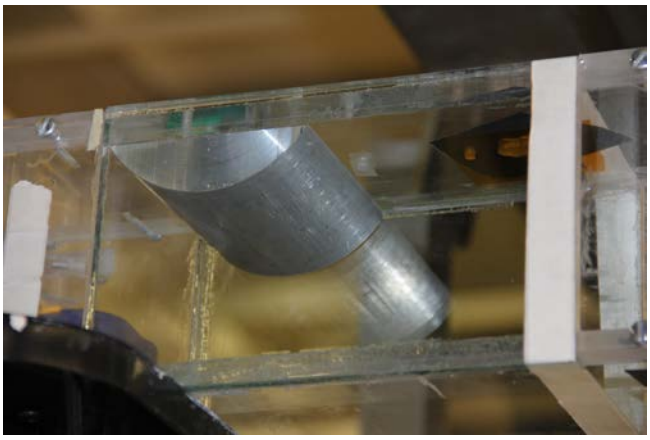

Figure 2. The cylindrical "slice" installed in the optical section.

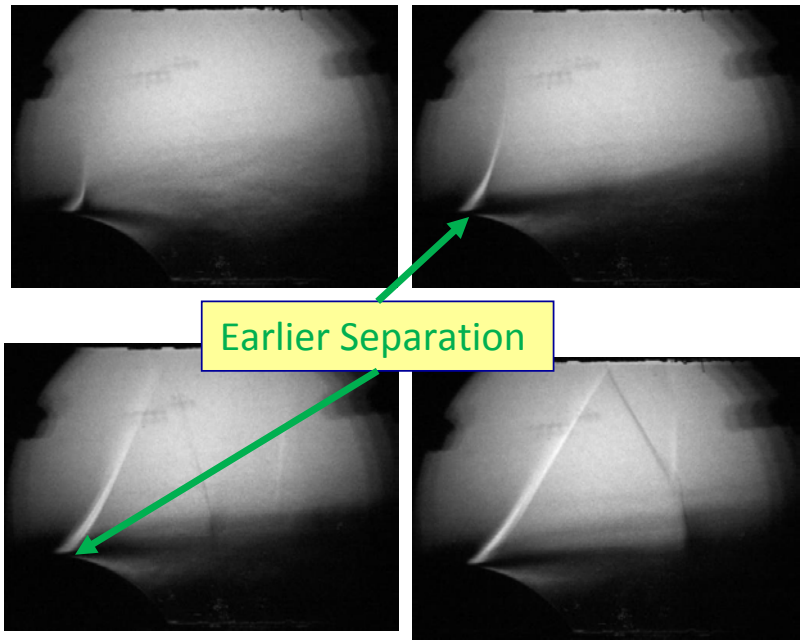

Figure 3. Flow topology over the cylindrical "slice" at progressively increasing incoming Mach numbers, visualizing the formation and the evolution of the supersonic shock on the cylinder.

Although the main effort of this work was carried through experimental investigation, some computational simulations of the flow over the partially-protruding cylindrical "slice" were also performed using commercially-available Cobalt code. Results at different Mach numbers between 0.48 and 0.54 are presented in Figure 4. The flow topology and the shock evolution were found to be very similar to the experimentally observed topology, presented in Figure 3. Computational results predicted that the shock forms at the incoming M = 0.47, which is very similar to the experimentally measured value of M = 0.46. All these results demonstrate that the transonic flow around the partially-protruding cylindrical turret has many essential features observed around 3-dimensional turrets at transonic speeds, seen in Figure 1.

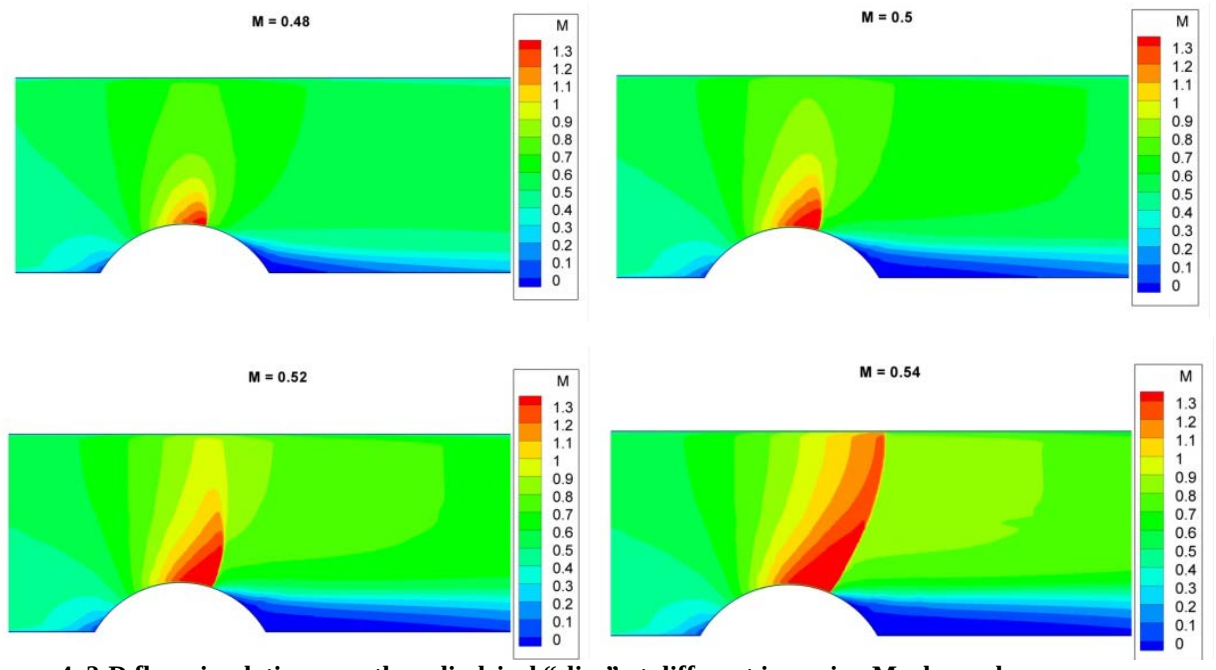

Figure 4. 2-D flow simulation over the cylindrical "slice" at different incoming Mach numbers.

III. Experimental Set-Up and Data Reduction

To investigate aero-optical effects around the cylindrical turret, a turret with a conformal window was designed and manufactured, see Figure 5. The turret is 100-mm long with a 103-mm diameter. The turret has a built-in set of optical elements, consisted of two off-the-shelf cylindrical lenses and a flat mirror, designed to reflect an incoming collimated beam with a minimum amount of optical distortions; that is, optically it is equivalent to an optical flat mirror. The optical aperture size is 30 mm along the streamwise direction and 50 mm in the spanwise direction. The outer curvature of the front cylindrical lens matches the curvature of the cylindrical turret.

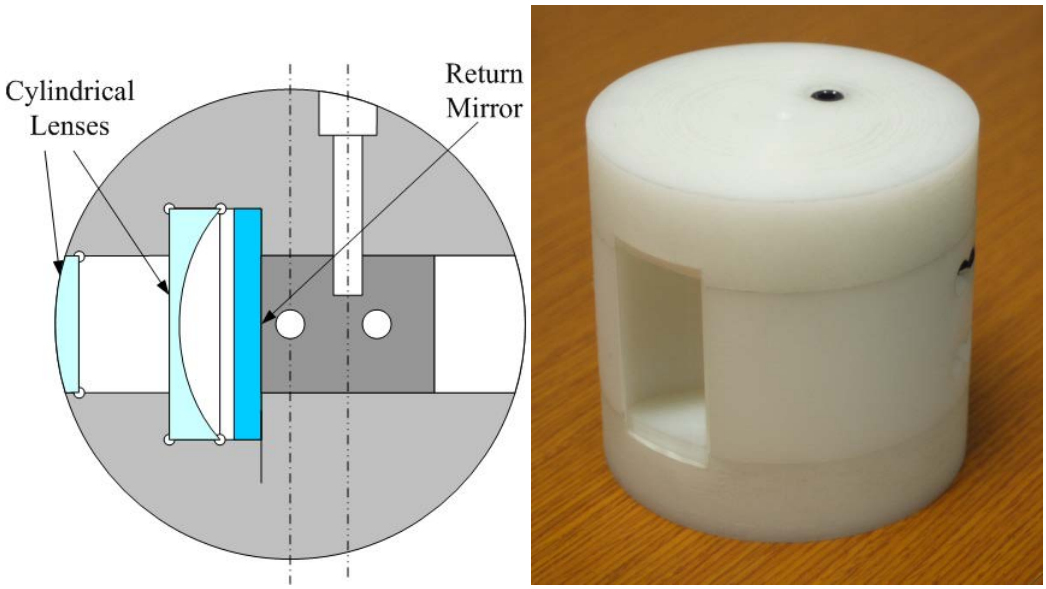

Figure 5. Cylindrical turret with a conformal window: drawing (left) and picture (right).

Preliminary investigation of the flow around the cylindrical "slice", discussed in the previous section, had shown that the wake downstream of the cylinder was unrealistically small and stable, compared to the wake

downstream of the 3-D turrets. To create a more-realistic wake downstream of the turret, a partially-protruding cylinder was tested in a test section with a back-step. This test section has a height jump, from 100 mm to 142 mm, at the location of the partially-protruding cylinder, see Figure 6 for picture and dimensional schematics of the test section. The cylinder protrusion was 7.5 mm for this test section. The test section was made of Plexiglas, except for the wall, through which the circular laser beam with a diameter of 40 mm was traversed, was made of glass to minimize steady optical distortions imposed on the laser beam. Aero-optical effects over a cylindrical turret of the same diameter with a flat window were tested in the same test section at moderate subsonic speeds and aero-optical distortions at back-looking angles were found to be very similar to ones observed over three-dimensional turrets [9].

The collimated laser beam was transmitted into the test section using steering mirrors. After the optical assembly inside the cylinder reflected it back along the same path, thus using a double-path approach and increasing the signal by factor of two, the returning beam was split aside and directed to a high-speed Shack-Hartmann wave-front sensor. The sensor sampling rate was 14 kHz with the spatial resolution of 30x60 subapertures, with 60 subapertures in the streamwise direction. Aero-optical measurements were collected over a range of transonic Mach numbers at an elevation angle of 105 degrees, with some limited measurements performed at 140 degrees. A Schlieren system was used to visualize the location and the strength of the local shock on top of the partially-protruding cylinder. The test section was also equipped with 9 static pressure ports, shown in Figure 6, located at the side wall of the test section to monitor the streamwise evolution of the flow speed along the test section.

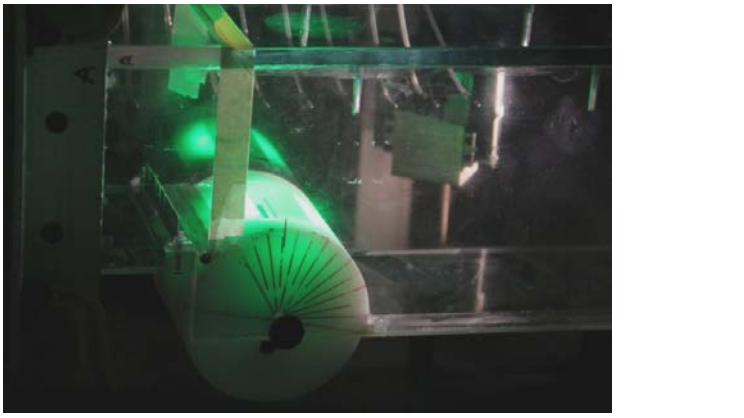

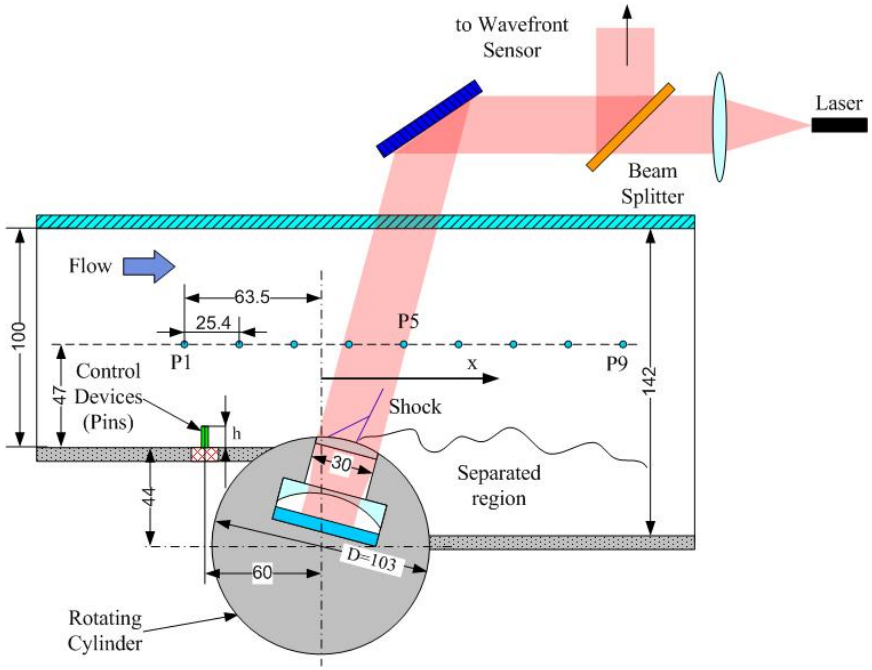

Figure 6. Picture (top) and schematic (bottom) of the optical set-up. All dimensions are in millimeters.

For each collected wavefront sequence, instantaneous tip/tilt and piston components from each wavefront were removed. The time-average wavefront, that is a steady lensing, was also removed from each wavefront. Wavefronts were normalized as,

$$WF_{Norm}\left(\frac{\mu m}{m}\right) = \frac{WF}{\frac{\rho}{\rho_{SL}} M^2 D},$$

where ρ is the free stream density, ρ_{SL} is the density at sea level, M is the Mach number at the port P1 at x/D = -0.625 and D is the turret diameter.

IV. Results

A. Shock dynamics for baseline case

The streamwise variation of the Mach number for different flow regimes for the baseline case (no flow control) are shown in Figure 7. Depending on the incoming speed, the flow had several regimes. At the incoming Mach number less than 0.6, the flow was subsonic everywhere around the turret. Then the incoming speed was increased to M = 0.63, a weak stationary shock was observed on top of the turret, see Figure 8, top left picture. When the incoming Mach number was increased slightly to 0.64, the shock became unsteady and was oscillating over the aperture between approximately 90 and 105 degrees, see Figure 8, top middle picture; this flow regime will be referred as a weak moving shock case. When the incoming Mach number was increased to 0.67, the shock continued oscillating over the aperture, with its strength and extent into the flow increased, see Figure 8, top left picture, a so-called strong moving shock case. At this point, when the plenum pressure was reduced to increase the incoming speed, the incoming Mach number was not changed, indicating that the flow was choked over the turret, see Figure 7; however, the flow speed continued increasing downstream of the turret and when it reached M = 1.1 at x/D=0.625, that is the pressure port P5, the shock became stationary, extending even further into the flow and anchored approximately at 105 degrees at the cylinder; this case later will be called a strong stationary shock case, see Figure 8, bottom left picture. When the plenum pressure was dropped to the minimum achievable value, the anchored location of the stationary shock moved further downstream and the shock was observed to be tilted more in the downstream direction, see Figure 8, bottom right picture.

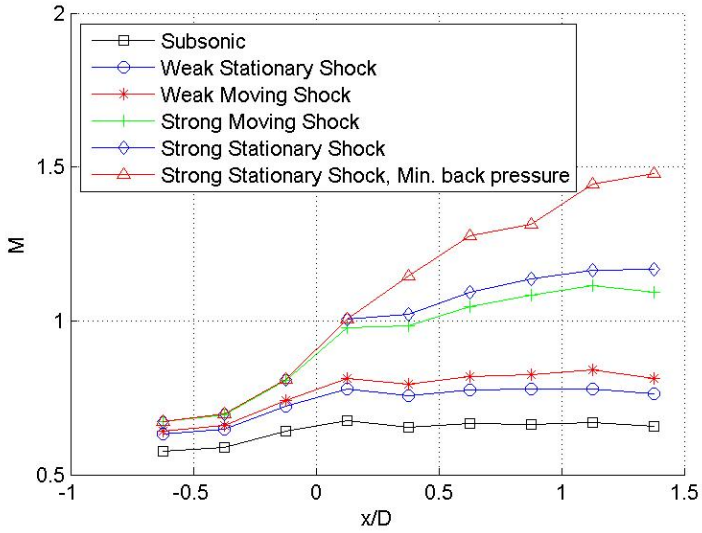

Figure 7. Streamwise evolution of Mach number for different shock strengths.

The shock-boundary-layer interaction leads to the flow separation immediately downstream the shock, which can be observed in the flow visualization in Figure 8. The shock location ultimately depends on the instantaneous pressure field over the turret. The shock-induced separation changes the pressure gradient immediately downstream the shock, and for cases where the relatively weak shock was formed over the region with small pressure gradients, such as the weak moving shock and the strong moving shock cases, the interaction between the shock and the shock-induced flow separation leads to unsteady pressure gradients downstream of the shock,

which results in the unsteady shock motion. A similar shock unsteadiness was observed over the hemisphere-on-cylinder turret at incoming transonic speed of 0.6 [14] and in the shock-induced separation on the wall of a slightly-overexpended supersonic nozzle [16]. When the shock becomes stronger, it is less-sensitive to the small wake-related pressure gradients downstream of it, thus becoming stationary. With the lowered back pressure, the shock and, consequently, the separation point moved downstream, in fact making the wake smaller for the stronger shock.

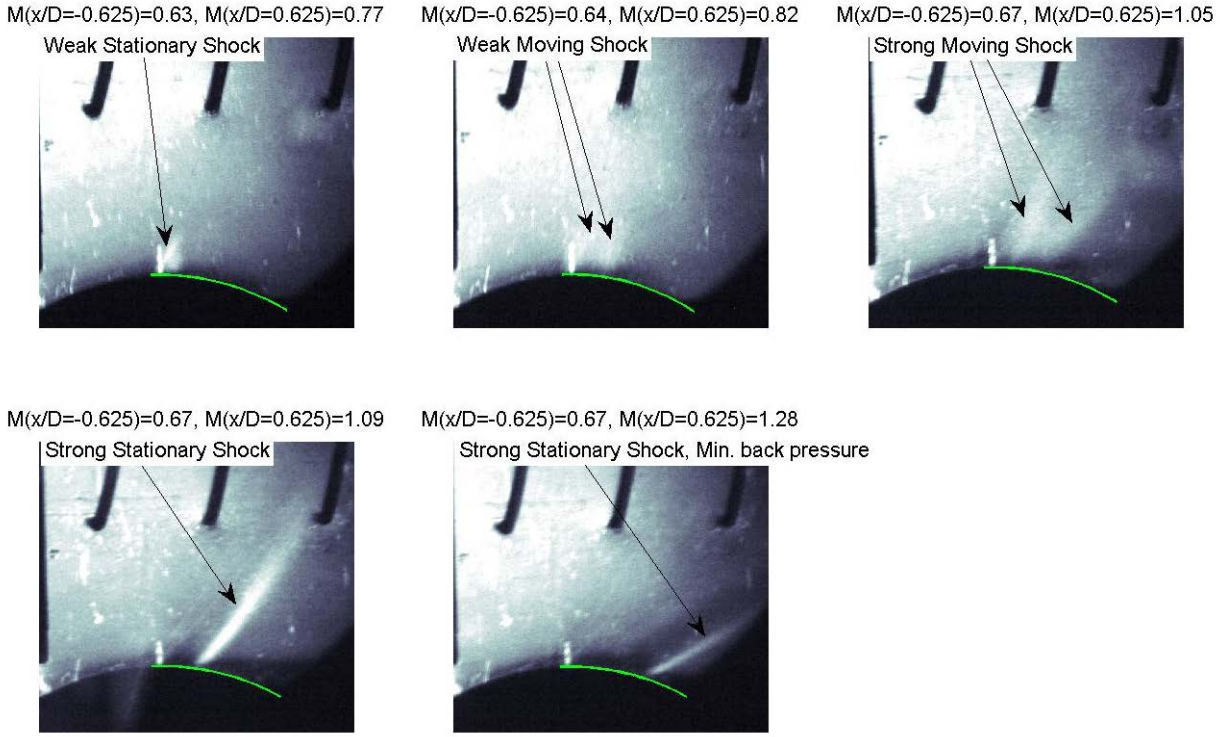

Figure 8. Long-exposure schlieren flow visualization for different flow regimes. The outline of optical aperture is labeled by a green line.

As a last comment, the shock formation and the spatial evolution with an increased Mach number over a partially-protruding cylinder in the back-step section was similar to the evolution observed for the flow over the cylindrical slice, Figures 3 and 4, with the main difference been the shock was observed to be visibly unsteady for the incoming Mach number between 0.64 and 0.67.

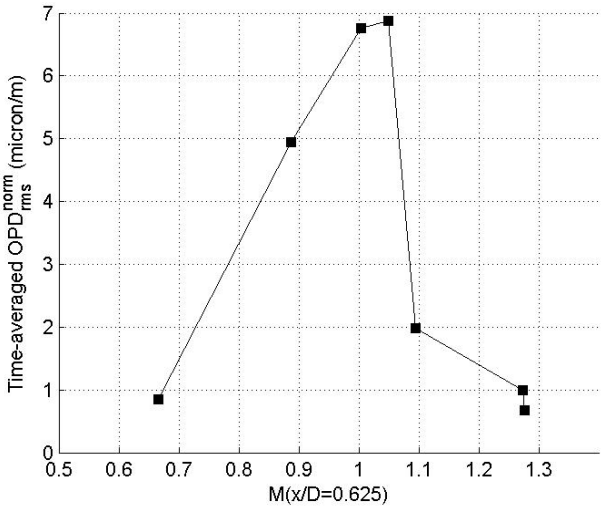

Figure 9. Normalized OPDrms for baseline for different regimes

The presence of the shock creates sharp pressure gradients and additional aero-optical distortions imposed on an outgoing beam. The level of aero-optical distortions is typically quantified by the time-averaged spatial root-mean-square of the wavefront over the aperture, $OPD_{rms} = \overline{\left\langle \sqrt{WF(\alpha,z,t)^2} \right\rangle}$. Baseline OPDrms for different flow regimes, normalized by $\frac{\rho}{\rho_{SL}} M^2 D$ are presented in Figure 9. For the subsonic case, the normalized OPDrms is approximately 1, which is very similar to values observed over hemispherical turret at the same elevation angle [14]. When the unsteady shock was formed over the aperture, OPDrms was dramatically increased a value of 5 for the weak moving shock case and reaching an even higher value of 7 for the strong moving case. But when the shock became stationary for higher Mach numbers, OPDrms dropped down to values 1-2, since the stationary wavefront was removed from all wavefronts, and OPDrms accounts only for the unsteady aero-optical component.

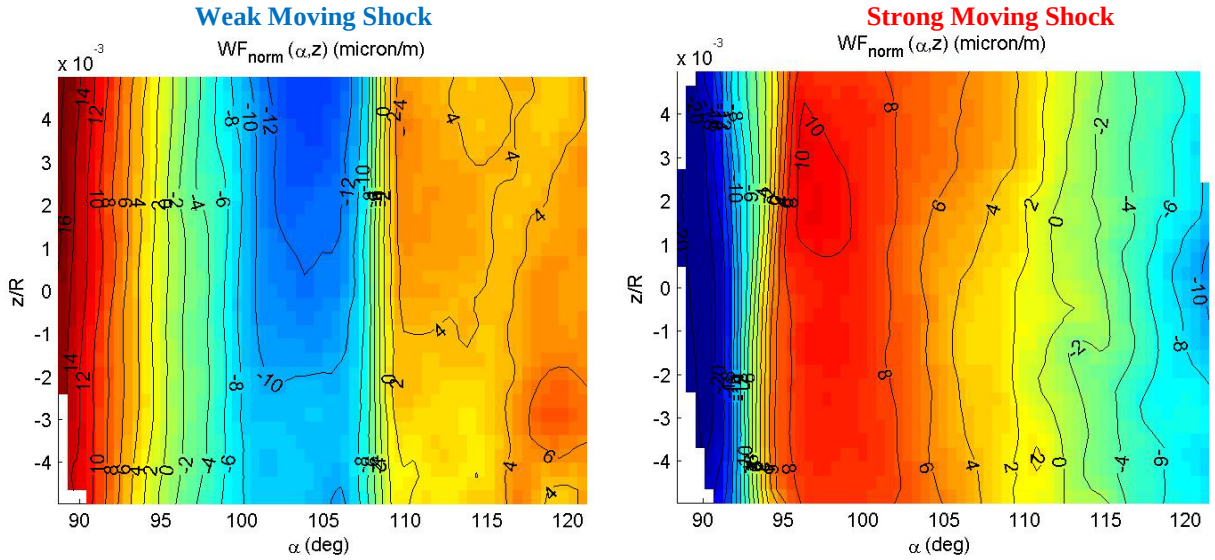

Figure 10. Individual wavefronts for the baseline case for different flow regimes. Flow goes from left to right.

Inspection of instantaneous wavefronts over the aperture for unsteady shock cases, with some of them shown in Figure 10, revealed that wavefronts and the shock were almost spanwise uniform. Thus, to simplify the further studies, one-dimensional streamwise wavefront slices through the center of the aperture in the spanwise direction, WF(α, z = 0, t), were extracted. Examples of the temporal evolution of the 1-D wavefront slices for three progressively increased incoming Mach numbers resulting in the unsteady shock are presented in Figure 11, along with instantaneous normalized values of OPDrms(t). The shock motion was observed to be fairly periodic with the normalized frequency of about 950 Hz; the similar shock-oscillating frequency was observed a weak shock over a three-dimensional turret [14]. One cycle of the wavefront sequence, marked in Figure 11 by two black lines for each Mach number are plotted in Figure 12 as 1-D wavefronts shifted in the vertical direction for clarity. The time instant for each wavefront time interval is normalized by the turret diameter and the incoming speed, $T = tU_\infty / D$. As the pressure and density increases across the shock, the wavefront exhibits a large positive jump across the shock and for each Mach number in Figure 12 the shock is indicated by the thick red line. The shock motion and instantaneous strength was found to very sensitive to the local flow speed. For the weak shock case, see Figure 12, left plot, the shock appeared around α = 105 degrees (moment T=3.31), quickly moved downstream to 110 degrees and gained additional strength (moments between 3.31 and 3.76), then quickly moved upstream and disappeared at moment T=4.21. Overall, the shock was present only during a relatively short time of approximately ΔT=1 out of ΔT=2.25 of the whole period. During other times the wavefront was relatively flat, resulting in relatively small values of less than 2 for the normalized OPDrms, see Figure 11, second plot from top.

In the case of the strong moving shock, see Figure 12, middle plot, the shock was present during the whole period, moving downstream and upstream between 95 and 112 degrees. The normalized OPDrms is this case was changing between values of 3 and 10, see Figure 11, fourth plot from top. For some instants the shock was observed

to momentarily gain strength and split into two weaker shocks, one moving upstream and another moving downstream on the aperture, see moments between T=11.64 and 11.95 in Figure 12, middle plot.

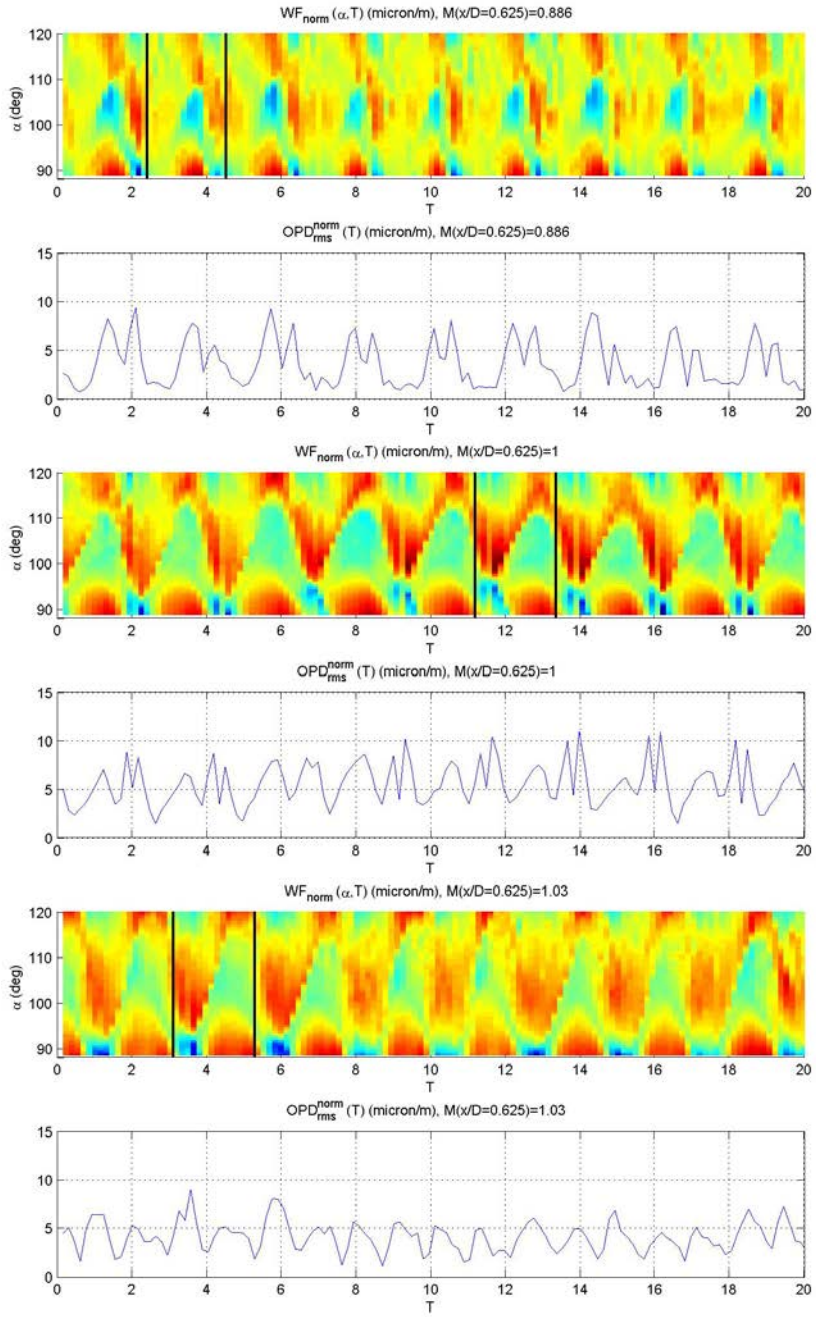

Figure 11. Temporal evolution of 1-D wavefronts and instantaneous normalized OPDrms for different local Mach numbers where the unsteady shock is present over the aperture. Wavefronts in time intervals marked by two solid black lines are re-plotted in Figure 12.

The temporal evolution of the shock in the strong moving shock case is very sensitive to the local Mach number. When the Mach number at the location x/D=0.625, pressure port P6, was slightly raised from 1.0 to 1.03, the shock was forming around 90 degrees and showed predominately downstream motion, see Figure 12, right plot. The apparent weakening of the shock strength when moving downstream on the aperture was probably due to the fact that the shock was mostly normal to the cylinder surface when it was located in the beginning of the aperture,

while it became more oblique by the end of the aperture, see Figure 8, top right picture, effectively reducing the gradient in the wavefront. As a consequence, instantaneous variations of the normalized OPDrms were reduced to be primarily between 2 and 5, see Figure 11, bottom plot.

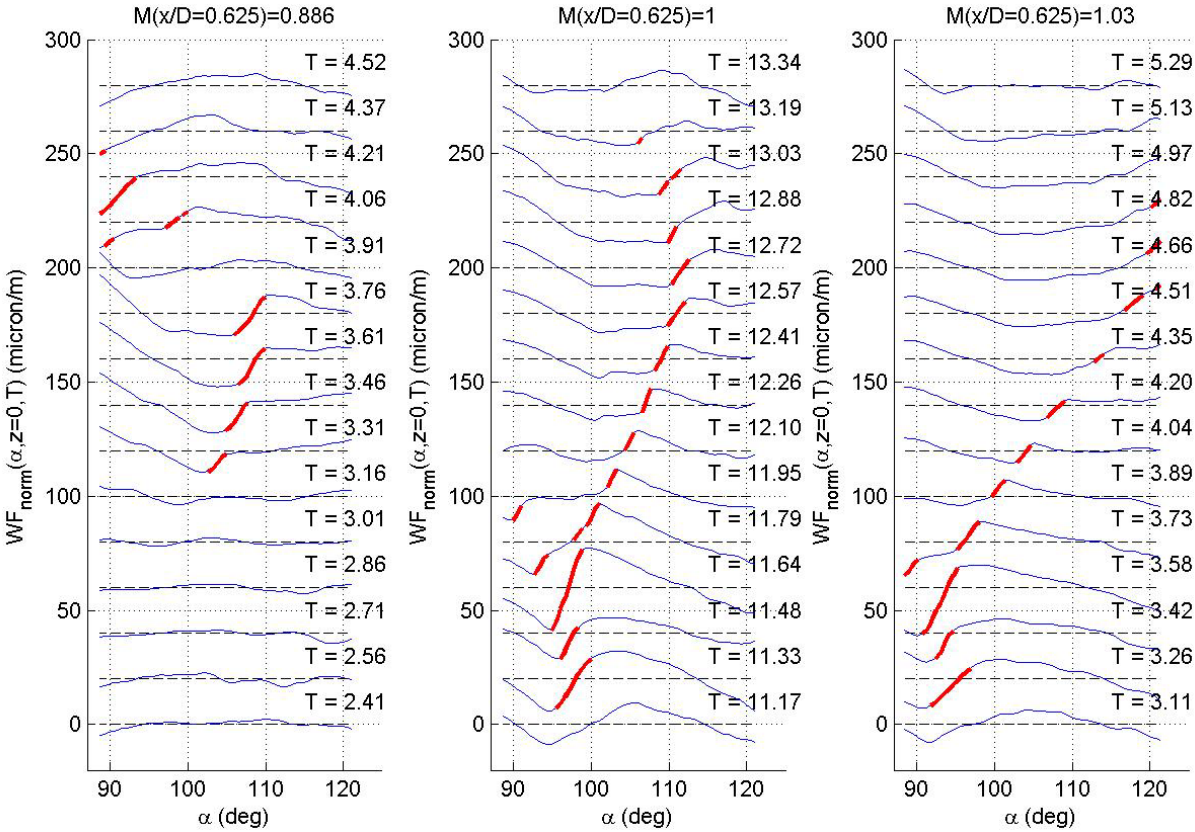

Figure 12. One-dimensional wavefronts during one period of the shock oscillation at different local Mach numbers, corresponding to the weak unsteady shock (left) and the strong unsteady shock with two different local Mach numbers (middle and right). Wavefronts are shifted in the vertical direction for clarity, the shock is marked by a thick red line.

B. Flow around passive flow devices

In addition to a study of the baseline, the effect of different passive flow control devices placed upstream of the turret on aero-optical aberrations over a partially-protruding cylindrical turret at different transonic speeds were investigated. The passive devices were a spanwise row of vertical pins with different heights, diameters and spacing placed on the tunnel wall shortly upstream of the turret, see Figure 6. Also a spanwise porous vertical screen was tested. All tested configurations are shown in Figure 13 and relevant parameters are provided in Table 1. The blockage, β, is defined as ratio between solid area and overall area, for pins it is $\beta = d/L$.

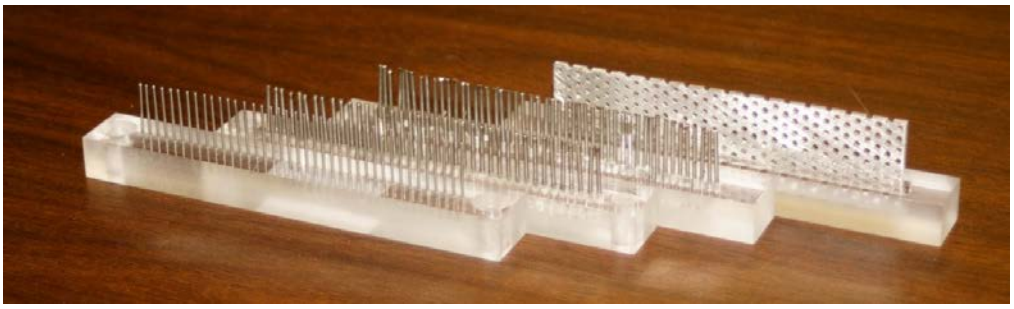

Figure 13. Passive flow control devices.

Table 1. Tested configurations

Configuration	Diameter d (mm)	Spacing L (mm)	Height h (mm)	Blockage β
Baseline	0	0	0	0
Pin1	0.87	2.5	15	0.35
Pin2	1.3	2.5	13	0.52
Pin3	1.25	2	15	0.62
Screen	-	-	17	0.78

Pins placed upstream of the partially-protruding cylinder were shown to be effective in reducing aero-optical effects over the cylindrical turret at subsonic speeds at earlier studies [11]. Pins introduce fine-scale turbulence, which increases total pressure losses and slows the flow downstream of pins. To quantify this effect, passive flow control devices were placed on the floor of empty test section with 100 mm x 100 mm square area and u-component velocity profiles were measured at several downstream locations using a hot-wire mounted on a computer-controlled traverse system, schematically shown in Figure 14. The incoming Mach number was 0.4.

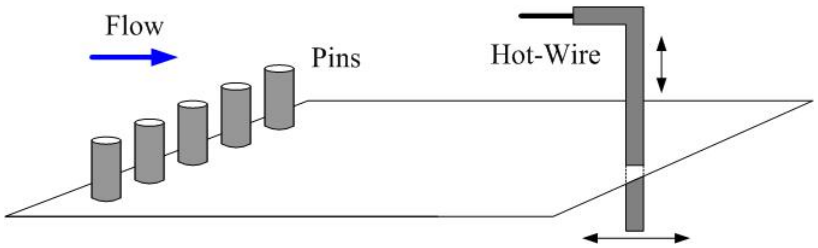

Figure 14. Schematics of velocity measurements downstream of a passive control device using a single hot-wire.

Cross-stream velocity profiles, both the mean and the fluctuating component, for the baseline and for all tested devices 50 mm downstream of the device are presented in Figure 15. All devices significantly reduced the mean speed downstream of them and the amount of the speed reduction was monotonically increasing with the increasing blockage value, to as low as 0.2 of the freestream speed for the screen; the velocity fluctuations in the low-speed region was small, less than 5% of the freestream velocity. The low-speed region extended roughly the height of the device away from the wall and the shear layer formed between the low-speed and the high freestream speed, with the fluctuating velocity increasing inside the shear layer. The shear layer strength was monotonically increasing for larger-blockage devices. Analysis of the shear layer spreading rate had shown that the shear layer grew approximately at the same rate as canonical shear layers, $\frac{d\delta_\omega}{dx} \approx 0.18\frac{U_{high}-U_{low}}{U_{high}+U_{low}}$ [17], where δ_ω is the shear layer vorticity thickness and U_{high} and U_{low} are the high and low velocity values above and below the shear layer. Also the maximum fluctuation level inside the shear layer was found to be approximately $u_{rms}^{\max} = (0.13..0.17)\left(U_{high}-U_{low}\right)$, also consistent with values observed in canonical shear layers [18]. All these observations indicated that the flow downstream of the passive device can be modeled as a region of low-speed low-turbulence flow with an almost canonical shear layer forming along the interface between the low- and high-speed regions. Form here it follows that the low-flow region, L_{low}, will extend downstream of the device until the vorticity thickness will become roughly twice of the device height, $\frac{\delta_\omega}{L_{low}} \approx \frac{2h}{L_{low}} \approx \frac{d\delta_\omega}{dx} \approx 0.18\frac{U_{high}-U_{low}}{U_{high}+U_{low}}$, giving $L_{low} \sim 11h\frac{U_{high}+U_{low}}{U_{high}-U_{low}}$. For example, for the screen it gives $L_{low} \sim 15h$.

Using a potential model, developed to describe two-dimensional flow around porous screens in bounded channels [15], the value of the low speed and the location of the interface between the low-speed and the high-speed portion of the flow can be predicted if the pressure drop coefficient across the screen is known. Consequently, if the values of both the low- and high-speeds are known, the pressure drop coefficient can be estimated. The streamlines of the flow around Pin3 configuration are plotted in Figure 16, and experimental velocity profiles at several

streamwise locations are plotted in Figure 16, right plot, along with model-predicted velocity profiles. While the potential model cannot predict the formation of the turbulent shear layer, it does a good job predicting both the low- and the high-velocity values and the streamwise evolution of the shear layer location. Thus, this simple potential model could be useful to estimate the flow field downstream of passive flow devices, as the cylindrical surface can be easily included into the model using a panel method or a distrusted line of sinks/sources, for instance.

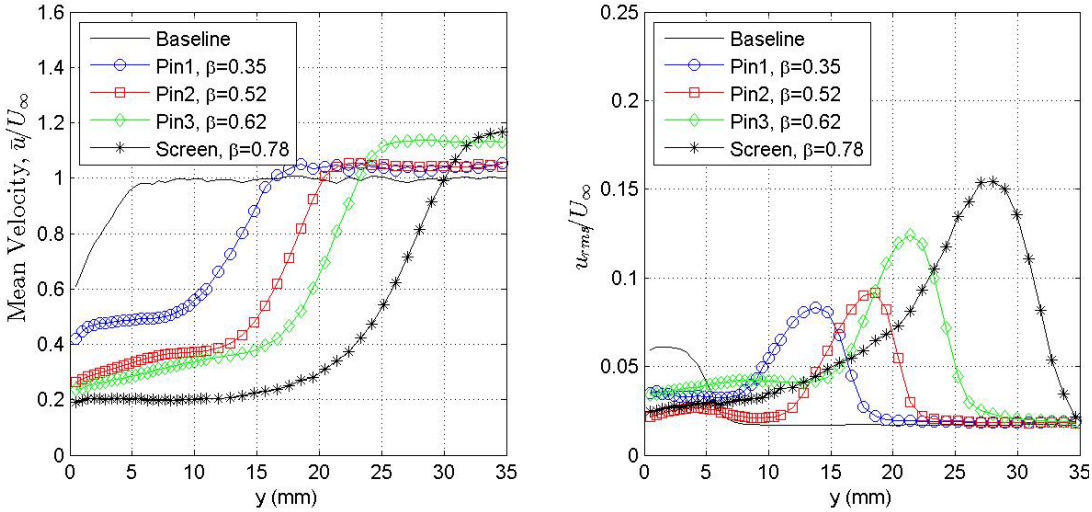

Figure 15. Profiles of mean U-velocity (left) and fluctuating U-component 50 mm downstream of the passive device.

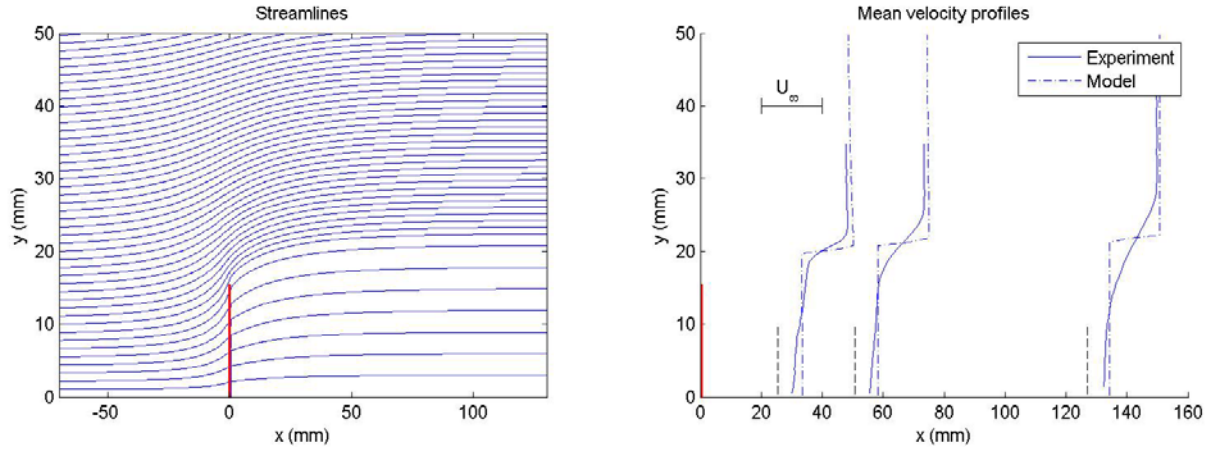

Figure 16. Left: Streamlines around Pin3 configuration computed using the potential model. Right: Mean velocity profiles at several locations downstream of Pin3 configuration, experimental results and model prediction. The device is marked by a thick red vertical line at x = 0, measurement locations are marked by dashed lines.

C. Aero-optical results for passive devices

Time-averaged levels of aero-optical distortions, OPDrms, for all tested configurations and speeds are presented in Figure 17. For subsonic case, all devices introduced an additional shear layer, progressively increasing aero-optical distortions with the increasing blockage value. For higher Mach numbers, Pin1 configuration did not slow the flow near the cylinder enough to eliminate the shock formation, but all higher-blockage devices pins eliminated the weak shock and therefore drastically reduced the level of aero-optical distortions at this elevation angle. Pin2 configuration, while not completely eliminating the shock formation at a higher incoming Mach number, which would correspond to the strong moving shock case for the baseline, did reduce the strength of the strong shock, therefore reducing the normalized OPDrms from 7 to 4. All higher-blockage devices completely eliminated the shock formation on the cylinder, but the formation of the secondary shear layer introduced additional aero-

optical distortions. This effect can be seen in Figure 17, as for the screen overall OPDrms values were consistently higher that for Pin3 configuration, which introduced a less-energetic shear layer, so overall level of the normalized OPDrms was less than 2 for all tested Mach numbers. Schlieren pictures of the baseline and Pin3 configuration for the incoming Mach number corresponding to the strong stationary shock case in the baseline are presented in Figure 18 and confirmed that pins eliminated the shock and introduced the secondary shear layer. Thus, there is an optimal blockage factor for passive flow control device, which does slow the flow near the cylinder surface enough to eliminate the shock formation, but does not introduce the strong shear layer over the cylinder, therefore minimizing the overall level of aero-optical distortions. Representative wavefronts for Pin3configuration corresponding to the weak and the strong moving shock cases are shown in Figure 19 and indeed showed the signs of the shear-layer structures.

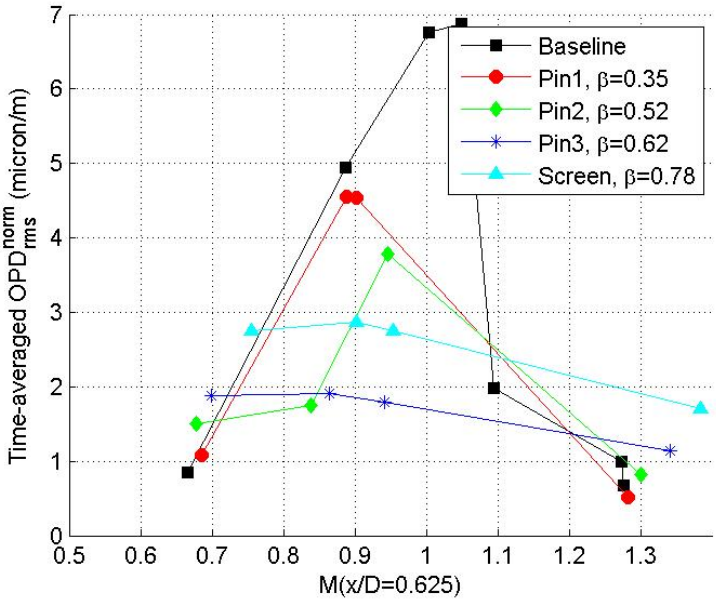

Figure 17. OPDrms for all tested configurations in the step section as a function of the local Mach number. Elevation angle is 105 degrees.

Figure 18. Flow topology for baseline (left) and Pin3 (right) for the strong stationary shock.

Overall, Pin3 configuration with the blockage value of 0.62 was found to be the best configuration to significantly reduce aero-optical levels around the partially-protruding cylinder at the elevation angle of 105 degrees at all tested speeds, except the subsonic speed, where it introduced additional shear-layer-related aero-optical distortions into the flow over the aperture.

Finally, aero-optical distortions for a larger elevation angle of 140 degrees were measured for the baseline and Pin1 configuration. For this angle, pins were found to be ineffective to modify the separation region and therefore, related aero-optical distortions. This result was somewhat expected, as the flow in the wake was subsonic

regardless, whether the shock was present on top of the cylinder or not, and Pin1 configuration was previously shown to be ineffective in reducing OPDrms at subsonic speeds for large elevation angles [11].

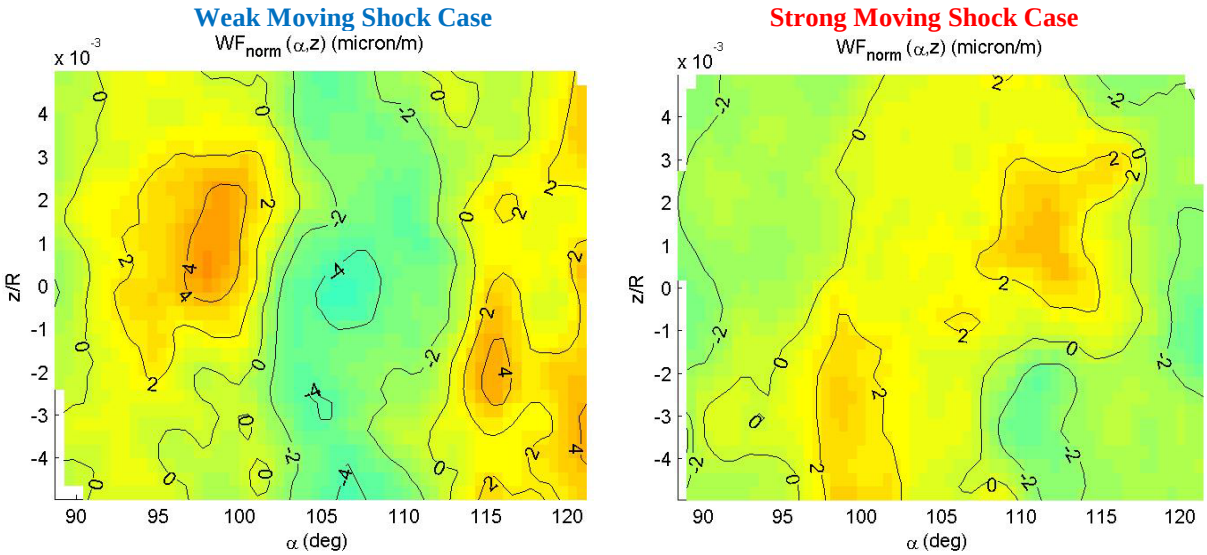

Figure 19. Individual wavefronts for the Pin3 configuration for different flow regimes. Flow goes from left to right.

Thus, passive devices as rows of tall thin pins or vertical screen with large blockage values were found to be effective in eliminating the local shock on top of the cylindrical turret by introducing fine-scale turbulence and related pressure losses near the surface of the turret and ultimately reducing the local speed to subsonic speed. This results in a drastic reduction of aero-optical shock-related effects. Pins were found to be ineffective to manipulating the wake downstream of the cylinder.

V. Conclusions and discussion

Extensive experimental studies were performed to quantify aero-optical effects around the partially-protruding cylinder at a wide range of transonic speeds to study shock-related effects on aero-optical distortions. Different transonic flow regimes, related local shock topology and dynamics were visualized and described using a Schlieren system. Highly-resolved, both in time and space, aero-optical measurements of the baseline flow (no flow control) and with various pins or screen configurations, placed upstream of the cylindrical turret, were performed at different incoming speeds. The baseline shock dynamics was found to be very sensitive to the local speed over the cylinder, exhibiting either a highly-unsteady or a fairly-steady shock near the cylindrical surface.

Pins were found to be a very promising candidate for controlling shock dynamics, as they significantly reduced aero-optical distortions when the beam was transmitted through the shock region for different shock strengths by either eliminating or significantly weakening the shock on top of the turret. Pins were found largely ineffective in modifying the separation region downstream of the shock.

In addition, limited steady-state computational simulations of the flow around both the cylindrical and hemispherical turrets at different incoming transonic speeds were performed and it was shown that the shock topology and dynamics over the cylindrical turrets is very similar to the shock topology and evolution with incoming speed over the hemispherical turret.

Based on the presented results, several viable candidates, namely a spanwise row of vertical pins or a vertical screen, were tested and were shown to successfully mitigate the shock and related aero-optical effects present on top of the cylindrical turret. The physical mechanism of how pins mitigate the shock was found to be total pressure losses introduced by pins into the flow near the surface of the turret and the blockage value was shown to uniquely quantify the device effect of the flow. The potential model was shown to satisfactory explain main features of the flow downstream of devices. As devices introduce additional shear layer into the flow, there is an optimum value of the blockage value around 0.6, which results in the largest reduction in aero-optical distortions.

To increase the pressure losses, multiple spanwise rows of pins should be explored in the future to see whether they can further improved aero-optical, shock-related distortions by transonic flow around turrets. Also, a

hybrid approach, consisting of a passive device (pins) to weaken the shock over the turret combined with other passive or active flow control to eliminate the wake behind the cylindrical turret might be the next step in further mitigating aero-optical effects at transonic speeds over a large range of elevation angles.

The presented work was performed in a wall-boundary flow, thus creating additional tunnel-blockage effects, like the flow chocking at some incoming Mach number and supersonic freestream speed downstream of the turret for the low plenum pressure, which will not be present in unbounded flows; undoubtedly, additional studies should be performed to further understand the differences between the wall-bounded and unbounded transonic flows. However, the authors believe that the results presented in this paper are generic enough to show promising passive-flow-control candidates to eliminate very detrimental, unsteady-shock-related aero-optical effects by keeping the flow subsonic everywhere around the turret. The described potential model, with some modifications to account for three-dimensional effects, can be used to optimize pins' location, height and the blockage value on the hemispherical turret in order to eliminate shock-related effects over a wide range of transonic numbers. In addition, proposed devices can be easily integrated with other passive/active flow control devices, potentially further improving aero-optical distortions at transonic speeds.

Acknowledgments

This work was funded by the Air Force Research Laboratory, Directed Energy Directorate. The U.S. Government is authorized to reproduce and distribute reprints for governmental purposes notwithstanding any copyright notation thereon.

References

[1] S. Gordeyev and E. Jumper, "Fluid Dynamics and Aero-Optics of Turrets", *Progress in Aerospace Sciences*, **46**, (2010), pp. 388-400.

[2] Gilbert, K. G. and Otten L. J. (eds), "Aero-Optical Phenomena," *Progress in Astronautics and Aeronautics*, Vol. 80, pp. 1-9, AIAA, New York, 1982.

[3] M. Weng, A.Mani and S. Gordeyev, "Physics and Computation of Aero-Optics", *Annual Review of Fluid Mechanics*, Vol. **44**, pp. 299-321, 2012.

[4] C. Porter, S.Gordeyev, M. Zenk and E. Jumper, "Flight Measurements of Aero Optical Distortions from a Flat-Windowed Turret on the Airborne Aero-Optics Laboratory (AAOL)", AIAA Paper 2011-3280, 2011.

[5] N. De Lucca, S. Gordeyev and E. Jumper, "The Airborne Aero-Optics Laboratory, Recent Data", Acquisition, Tracking, Pointing, and Laser Systems Technologies XXVI, Proceedings of SPIE, Volume 8395, Paper 8395-7, June, 2012.

[6] B. Vukasinovic, A. Glezer, S.Gordeyev, E. Jumper and V. Kibens, "Hybrid Control of a Turret Wake," *AIAA Journal*, Vol. **49**, No. 6, pp. 1240-1255, 2011.

[7] M. Palaviccini, L. Cattafesta and B. George," Passive Flow Control over a Three-Dimensional Turret with a Flat Aperture", AIAA Paper 2011-3265, 2011.

[8] B. Vukasinovic, A. Glezer, S. Gordeyev, E. Jumper and V. Kibens, "Active Control and Optical Diagnostics of the Flow over a Hemispherical Turret", AIAA Paper 2008-0598, 2008.

[9] S. Gordeyev, J.A. Cress, E. Jumper and A.B. Cain, "Aero-Optical Environment Around a Cylindrical Turret with a Flat Window", *AIAA Journal*, Vol. **49**, No. 2, pp. 308-315, 2011.

[10] S. Gordeyev, E. Jumper, T. Ng and A. Cain, "The Optical Environment of a Cylindrical Turret with a Flat Window and the Impact of Passive Control Devices", 36th, AIAA Paper 2005-4657, 2005.

[11] S.Gordeyev, J. Cress, A. Smith and E. Jumper, "Improvement in Optical Environment over Turrets with Flat Window Using Passive Flow Control", AIAA Paper 2010-4492, 2011.

[12] K. Wang, M. Weng, S. Gordeyev and E. Jumper "Computation of Aero-Optical Distortions over a Cylindrical Turret with Passive Flow Control", AIAA Paper 2010-4498, 2010.

[13] S. Gordeyev, E. Jumper, T. Ng and A. Cain, "Aero-Optical Characteristics of Compressible, Subsonic Turbulent Boundary LayerAIAA Paper 2003-3606, 2003.

[14] N. De Lucca, S. Gordeyev and E. Jumper, "Comparison of Aero-Optical Measurements from the Flight Test of Full and Hemispherical Turrets on the Airborne Aero-Optics Laboratory", AIAA Paper 2012-2985, 2012.

[15] J.-K. Koo and D.F. James, "Fluid flow around and through a screen", *Journal of Fluid Mechanics*, Vol. **60**, part *3*, pp. 513-538, 1973.

[16] B.J. Olson and S.K. Lele,"Large-Eddy Simulation of an over-expanded planar nozzle", AIAA Paper 2011-3908, 2011.

[17] Brown, G. L. and Roshko, A,"On density effects and large structure in turbulent mixing layers", *J. Fluid Mech.***64**, pp. 775-816. 1974.
[18] Rogers, M. M. and Moser, R. D.,"Direct simulation of a self-similar turbulent mixing layer", *Phys. Fluids,***6**, pp. 903-923, 1994.